Fibers and Polymers 2016, Vol.17, No.8, 1131-1139
DOI 10.1007/s12221-016-6529-1

ISSN 1229-9197 (print version)
ISSN 1875-0052 (electronic version)

Polyacrylic Acid-grafted Magnetite Nanoparticles for Remediation of Pb(II)-Contained Water

Xiaoyu Guan, Sunxian Yan, Qi Zeng, Zhou Xu[1], Yi Chen*, and Haojun Fan

Key Laboratory of Leather Chemistry and Engineering of Ministry of Education, Sichuan University, Chengdu 610065, P. R. China
[1]*Solid-state Fermentation Resource Utilization Key Laboratory of Sichuan Province, Yibin University, Yibin 644007, P. R. China*

(Received May 15, 2016; Revised July 16, 2016; Accepted July 22, 2016)

Abstract: Toxic Pb(II) contaminants in water pose a significant threat to the environment and public health, and thus technologies for Pb(II) remediation are attracting increasing industrial interests. In the present work, polyacrylic acid, offering abundant carboxyl groups capable of coordination with Pb(II) cations, was grafted from the magnetite nanoparticle surface *via* the bridging function of silane coupling agent for remediation of Pb(II)-contained water. Multiple techniques were employed to characterize the structure of the nanocomposite, and the effects of nanoadsorbent dose, pH value, and temperature on Pb(II) removal capability of the nanocomposite were investigated, respectively. Furthermore, adsorption kinetics and isotherms studies were performed for better understanding the mechanism by which Pb(II) cations were adsorbed. Finally, the feasibility of regenerating the exhausted nanoadsorbent by simply changing pH value was explored. According to these results, we intend to offer an efficient, separable, and reusable magnetic nanoadsorbent that may be a potential candidate for remediating Pb(II) contamination in water.

Keywords: Polyacrylic acid, Magnetite, Nanocomposite, Adsorption, Pb(II)

Introduction

Heavy metal ions in industrial wastewater and natural water, due to their toxicity and bioaccumulation through the food chain, pose a significant threat to environment and, thus, human health. Among various heavy metal ions, lead ion (Pb(II)) is believed to be a dominating contaminant, the hazardous effects of which have been documented since ancient Rome. Exposure to water with even a low concentration of Pb(II) can give rise to toxic effects that may suppress cellular activities, and hence arouse a variety of cancers [1-3]. With fast industrialization and modernization all over the world, the perniciousness of Pb(II) to human beings will persist, if not worsen, in the short run. Over the past few decades, significant efforts were directed to explore technologies for Pb(II) removal from aqueous solution, such as ion exchange [4], chemical precipitation [5], membrane-based process [6], and adsorption [7]. Of these effectual technologies, adsorption exhibits both economic and operational feasibility by virtue of its versatile adaptability, cost effectiveness as well as easy regeneration [8,9].

Ever since 1950s, it has been demonstrated that materials that range from approximately 1 to 100 nanometers in at least one dimension have distinct advantages over traditional bulk materials, which has been attracting increasingly extensive attention for both fundamental research and practical applications [10-15]. On the one hand, the extremely small size, and thus high specific surface area of nanoscale materials are propitious for interface-related applications, such as adsorption or catalysis. On the other hand, the surface chemistry of nanoscale materials proves tunable, yielding nanocomposite manifesting fundamentally new functions or emergent properties unattainable in traditional composites. Recently, magnetite-supported nanomaterials have attracted extensive interests in diverse fields. By decorating the magnetite surface with different functional materials, the resultant nanocomposite can be manipulated conveniently by using an external magnetic field. This so-called "remote control" or "action at a distance" has currently found a broad spectrum of possible applications, including electronics, catalysis, enzyme immobilization, targeted drug delivery, magnetic resonance imaging, and environmental remediation [16-21]. One compelling example is that of magnetite nanoparticles surface-grafted with poly(*N*-acryloyl ciprofloxacin-*co*-acrylic acid), which were reported as a magnetically-recoverable nanocomposite potentially applicable for microbial decontamination of collagen solution [19]. In addition, Feng *et al.* explored the feasibility of using polyhydroquinone-coated magnetite as a recyclable catalyst for degradation of flumequine in aqueous solution [20].

In this study, polyacylic acid was grafted from vinyl-silane modified magnetite nanoparticle surface *via* free radical polymerization, in an attempt to design a nanoadsorbent potentially applicable for remediating Pb(II)-contained water. Multiple techniques were employed to characterize the structure of the nanoadsorbent, and the effects of nanoadsorbent dose, pH value, and temperature on Pb(II) removal capability of the nanoadsorbent were investigated, respectively. Furthermore, adsorption kinetics and isotherms

*Corresponding author: chenyi_leon@scu.edu.cn

studies were performed for better understanding the mechanism by which Pb(II) cations were adsorbed. Finally, the feasibility of regenerating the exhausted nanoadsorbent by simply changing pH value was explored. Based on these results, we intend to offer an efficient, separable, and reusable magnetic nanoadsorbent that may be an addition to the ongoing fight against Pb(II) contamination in water.

Experimental

Materials

Ferric chloride ($FeCl_3$, reagent grade, purity ≥ 98.0 %), ferrous chloride dihydrate ($FeCl_2·2H_2O$, ACS reagent, purity ≥ 99.5 %), ammonium hydroxide solution ($NH_3·H_2O$, ACS reagent, 25.0-30.0 % NH_3 basis), and anhydrous ethanol (CH_3CH_2OH, reagent grade, purity ≥ 99.5 %) were purchased from Cheng Jie Chemical Engineering Co. Ltd. (Shanghai, China). Methacryloxy propyl trimethoxyl silane (MPTMS, deposition grade, purity ≥ 99 %) and toluene (C_7H_8, analytical grade, purity ≥ 99.5 %) were available from Sigma-Aldrich (Shanghai, China). Furthermore, *N*,*N*-dimethyl formamide (DMF, analytical grade, purity ≥ 99.5 %), anhydrous acrylic acid (AA, recrystallized from chloroform before use, purity ≥ 99.5 %), azobisisobutyronitrile (AIBN, recrystallized from methanol before use, purity ≥ 99 %), sodium hydroxide (NaOH, reagent grade, purity ≥ 98.0 %), nitric acid (HNO_3, reagent grade, purity ≥ 98.0 %), and lead nitrate ($Pb(NO_3)_2$, analytical grade, purity ≥ 99.5 %) were obtained from Kelong Chemical Engineering Co. Ltd. (Chengdu, China).

Preparation of Fe_3O_4 Nanoparticles

Fe_3O_4 nanoparticles were synthesized according to a slightly modified version of a previously published protocol [22]. Briefly, $FeCl_3$ (2.8 g) and $FeCl_2·2H_2O$ (1.6 g) were dissolved in nitrogen-purged ultrapure water (18.2 MΩ·cm at 25 °C) to yield a mixture, where the molar ratio of Fe^{3+} and Fe^{2+} cations approximated to 1.75:1. Then, NH_3 aqueous solution (25.0-30.0 % NH_3 basis) was added dropwise until the pH value reached 10. After incubated at 85 °C for 30 min, the black Fe_3O_4 precipitations were magnetically separated and washed with anhydrous ethanol for five times. Finally, the product was dried in a vacuum oven at 60 °C until a constant weight.

Vinyl-silane Modification of Fe_3O_4 Nanoparticles

To facilitate polyacrylic acid (PAA) grafting from the magnetite nanoparticle surface, the magnetite nanoparticles prepared above were modified by vinyl-terminated silane coupling agent first. Typically, 2 g Fe_3O_4 and 250 m*l* toluene were added into a three-necked flask equipped with a flowing nitrogen atmosphere and a mechanical stirrer. After mechanical stirring at ambient temperature for 30 min, 4 m*l* MPTMS was added in batches and then the temperature was elevated up to 80 °C for incubation. After 10 h, the engineered magnetite nanoparticles, referred to as Fe_3O_4/MPTMS, were isolated from the solution by using a magnet, washed five times with anhydrous ethanol, and dried at 70 °C.

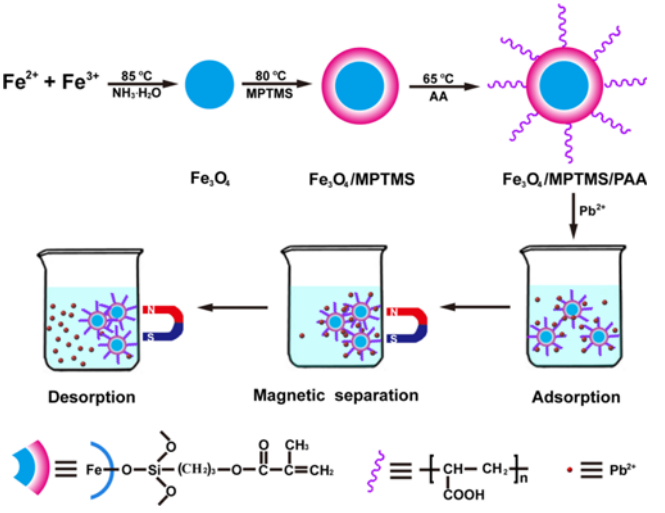

Scheme 1. Synthesis of Fe_3O_4/MPTMS/PAA nanocomposite and its application for Pb(II) removal from aqueous solution.

Synthesis of Fe_3O_4/MPTMS/PAA Nanoparticles

PAA-functionalization of Fe_3O_4/MPTMS nanoparticles was carried out according to the following procedure. In brief, 1 g Fe_3O_4/MPTMS, 150 m*l* DMF, 2 m*l* AA, and 0.02 g AIBN were added into a 250 m*l* three-necked flask. Free radical polymerization was then carried out at 65 °C under an atmosphere of nitrogen. After 8 h, the reaction was quenched by cooling the system to room temperature. The magnetic nanocomposite obtained, referred to as Fe_3O_4/MPTMS/PAA, was separated with a magnet and washed repeatedly with ultrapure water to remove any excess AA, PAA from self-polymerization and/or AIBN. The synthesis procedure and the structure of the product are illustrated in Scheme 1.

Structural Characterization of Fe_3O_4/MPTMS/PAA Nanoparticles

SEM images were taken on a JEOL JSM-7500F (Japan) field emission scanning electron microscope operated at an accelerating voltage of 5.0 kV. TEM specimens were observed on a JEOL JEM-2010 transmission electron microscope (Japan) at an accelerating voltage of 200 kV. Brunauer-Emmitt-Teller (BET) specific surface area was measured by low-temperature nitrogen adsorption/desorption experiments, conducted on a Micromeritics ASAP 2020 Accelerated Specific Surface Area and Porosimetry Analyzer (United States). X-ray photoelectron spectra (XPS) measurement was conducted on a Kratos XSAM800 system (Britain) with Al-Kα radiation (1486.6 eV) in the constant analyzer energy mode. During data acquisition, all the binding energies were

calibrated based on the hydrocarbon C1s peak set at 284.6 eV. Total organic carbon (TOC) content was measured by using an Apollo 9000 TOC/TN auto analysis system (Tekmar-Dohrmann, United States). XRD patterns were collected on a Philips X'Pert pro MPD diffractometer equipped with a copper anode producing X-rays with a wavelength of 1.5406 Å in the range of 2θ=10-80 °. A model No. 735 vibrating sample magnetometer (VSM, NanJing, China) with a magnetic field of ±10 kOe was employed to determine the magnetization of the magnetic nanoparticles.

Pb(II) Adsorption and Desorption Experiment

Aqueous Pb(II) stock solution with different concentrations were prepared by dissolving a predetermined quantity of $Pb(NO_3)_2$ in ultrapure water. Batch Pb(II) adsorption studies were carried out by mixing a predetermined amount of Fe_3O_4/MPTMS/PAA with a certain volume (25 m*l*) of Pb(II) aqueous solution held in a 100-m*l* Erlenmeyer flask. The mixture was subject to ultrasonic oscillation for 2 min, and then shaken at 200 rpm in a thermostatic orbit incubator to reach equilibrium. The impact of nanoadsorbent dose, pH value, and temperature on Pb(II) removal capacity of Fe_3O_4/MPTMS/PAA were investigated, respectively. After a predetermined adsorption time, the nanoparticles were separated temporarily by using a magnet, and 1 m*l* of the residual solution was withdrawn by a syringe. In order to measure the residual concentration of Pb(II) by inductively coupled plasma-optical emission spectroscopy (ICP-OES, Optima 2100 DV, Perkin-Elmer Instruments, United States), the solution withdrawn was subject to traditional acid digestion first. Briefly, the withdrawn solution (1 m*l*) was introduced into a 100-m*l* Erlenmeyer flask containing 30 m*l* of ultrapure water and 2 m*l* of concentrated HNO_3, and then digested on a fuming cupboard at 100 °C until the volume of the solution decreased to approximately 10 m*l*. After that, 2 m*l* of H_2SO_4 aqueous solution (50 % v/v) was added and the digestion process continued for another 1 min. Finally, the digested solution was transferred into a 50-m*l* volumetric flask, diluted with ultrapure water to volume, and then filtered through a 0.2 μm cellulose acetate filter before ICP-OES measurement. Detailed experimental condition for Pb(II) adsorption experiment mentioned above were tabulated in Table S1. The amount of Pb(II) adsorbed per unit nanoadsorbent mass at time t (q_t) was calculated according to the following equation:

$$q_t = \frac{C_0 \times V_0 - C_t \times V_t}{m} \quad (1)$$

where C_0 (mg/*l*) and V_0 (*l*) are the initial concentration and volume (25 m*l*) of the Pb(II) solution, C_t (mg/*l*) and V_t (*l*) refer to the residual concentration and volume of the Pb(II) solution at time t, and m (g) represents the nanoadsorbent dose. In addition, the Pb(II) removal percentage at equilibrium was quantified by equation (2):

$$\% \text{ Removal} = \frac{C_0 - C_e}{C_0} \times 100 \quad (2)$$

where C_0 (mg/*l*) and C_e (mg/*l*) stand for the initial and equilibrium concentration of the Pb(II) solution, respectively.

To investigate the reusability of Fe_3O_4/MPTMS/PAA, the exhausted nanoadsorbent was regenerated by using a 0.1 M HNO_3 solution as the desorbent. Desorption of Pb(II) was carried out by mechanically stirring the exhausted nanoadsorbent in the HNO_3 solution for 45 min at 50 °C, and then the regenerated nanoadsorbent was washed thoroughly with ultrapure water until neutral. Subsequently, the regenerated nanoadsorbent was employed for Pb(II) removal from aqueous solution again, according to the methods described above. This desorption-adsorption procedure was repeated for five coherent recycles.

Results and Discussion

Structure of Fe_3O_4/MPTMS/PAA

Figure 1(a) presented the SEM image of native Fe_3O_4 nanoparticles. Clearly, they were roughly spherical in geometry with similar particle size, and piled up together after drying. The statistical size distribution of these Fe_3O_4 nanoparticles, which was obtained by cropping the SEM image *via* Image *J* software developed by National Institutes of Health (United States), was exhibited in Figure 1(b). The diameter of these native Fe_3O_4 nanoparticles averaged 19±1.5 nm, ranging from 13 to 26 nm. Furthermore, according to low-temperature nitrogen adsorption isotherm, these Fe_3O_4 nanoparticles possessed a specific surface area of 55.6±1.1 m^2/g. After surface grafting of PAA, the specific surface area of the nanocomposite decreased to 45.9±0.8 m^2/g. In spite of such decrease, the specific surface area of the nanocomposite was still so large that facilitated more Pb(II) adsorption and, thus, removal from aqueous solution. Figure 1(c) and (d) represented the TEM images of Fe_3O_4 and Fe_3O_4/MPTMS/PAA nanoparticles, respectively. In the case of Fe_3O_4/MPTMS/PAA, it was clear that the Fe_3O_4 nanoparticles, manifesting as dark contrast, were wrapped by a layer of light contrast. This observation indicated that a layer of polymer was successfully grafted from the Fe_3O_4 surface, yielding a typical core-shell structure as designed.

Whether PAA was successfully grafted from the engineered Fe_3O_4 nanoparticles as designed was further qualitatively verified by analyzing the XPS spectra of Fe_3O_4/MPTMS/PAA demonstrated in Figure 2. As could be seen in Figure 2(a), four elements, including Fe, Si, C, O, were detected in the XPS survey spectrum of Fe_3O_4/MPTMS/PAA nanocomposite. The high resolution XPS spectra of these four elements were further illustrated in Figure 2(b)-(e), respectively. In Figure 2(b), the photoelectron peak at 725.1 eV corresponded to the binding energy of Fe $2p_{1/2}$ in the Fe_3O_4 core, while the peak at 711.9 eV was attributed to Fe $2p_{3/2}$

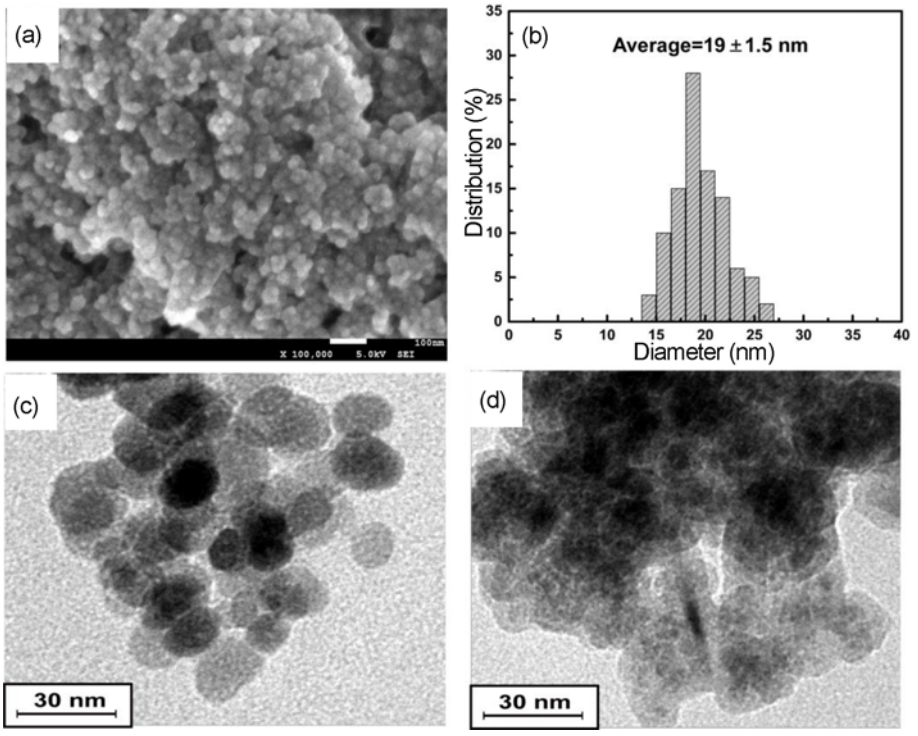

Figure 1. (a) SEM image, (b) size distribution of native Fe_3O_4 nanoparticles; TEM images of (c) Fe_3O_4 and (d) Fe_3O_4/MPTMS/PAA nanoparticles.

[19]. In addition, another XPS signal with relatively low intensity was found at 101.9 eV, corresponding to Si 2p component. This signal could only be ascribed to MPTMS derivative. The high resolution C 1s and O 1s core-level spectra, both deconvolved into four Gaussian components, were plotted in Figure 2(d) and (e), respectively. The C=O (288.6 eV/533.1 eV) and C-O (286.6 eV/531.4 eV) components could be assigned either to the ester from MPTMS or to those carboxyls from polyacrylic acid. In addition, the C-Si (284.1 eV) and Si-O (530.0 eV) components could only be ascribed to MPTMS derivative, while the Fe-O (530.0 eV) component stemmed from the Fe_3O_4 nanoparticle core. Furthermore, according to the theoretical carbon content (50.0 % (w/w)) in acrylic acid, as well as the total organic carbon (TOC) values in Fe_3O_4/MPTMS (168±2 mg/g) and Fe_3O_4/MPTMS/PAA (232±5 mg/g), it could be calculated that the Fe_3O_4/MPTMS/PAA nanocomposite roughly contained 12.8±0.3 % (w/w) of polyacrylic acid as the functional shell.

The crystalline structure and magnetic properties of Fe_3O_4/MPTMS/PAA nanocomposite were verified by XRD patterns and magnetic hysteresis loops, respectively. Figure 3(a) illustrated the XRD patterns of native Fe_3O_4, Fe_3O_4/MPTMS, and Fe_3O_4/MPTMS/PAA nanoparticles, respectively. In these three samples, the diffraction peaks observed could be indexed to the crystal planes of magnetic Fe_3O_4 nanoparticles. The peak positions and relative intensities were in good agreement with standard JCPDS data (75-0449), revealing the spinel structure of the co-precipitated Fe_3O_4 core [23,24]. In addition, a broad amorphous halo in the 2θ range from 20.0 ^{o} to 30.0 ^{o} appeared in both Fe_3O_4/MPTMS and Fe_3O_4/MPTMS/PAA nanoparticles, indicating the presence of MPTMS derivative and the PAA shell, which differed in morphology from the core. Figure 3(b) showed the magnetic hysteresis loops of Fe_3O_4 nanoparticles before and after surface modification. The hysteresis loops demonstrated the superparamagnetism of all three samples, because there was almost no coercivity once the magnetic field was removed. In addition, the saturated magnetization of native Fe_3O_4, Fe_3O_4/MPTMS, and Fe_3O_4/MPTMS/PAA nanoparticles was found to be 78.1, 40.8, and 18.9 emu/g, respectively. The decrease in saturation magnetization could be credited to decreased magnetite component after surface decoration [25,23]. In spite of such decrease, the magnetization of Fe_3O_4/MPTMS/PAA nanocomposite was still strong enough for them to be separated from aqueous solution by the aid of an external magnetic field. As shown in the inset of Figure 3(b), the Fe_3O_4/MPTMS/PAA nanocomposite could be magnetically recovered from aqueous solution within only 10 min, and as a result, the solution experienced a significant color change from black to transparent.

Pb(II) Removal Capability of Fe_3O_4/MPTMS/PAA

The influence of nanoadsorbent dose on Pb(II) removal by Fe_3O_4/MPTMS/PAA was presented in Figure 4(a). According

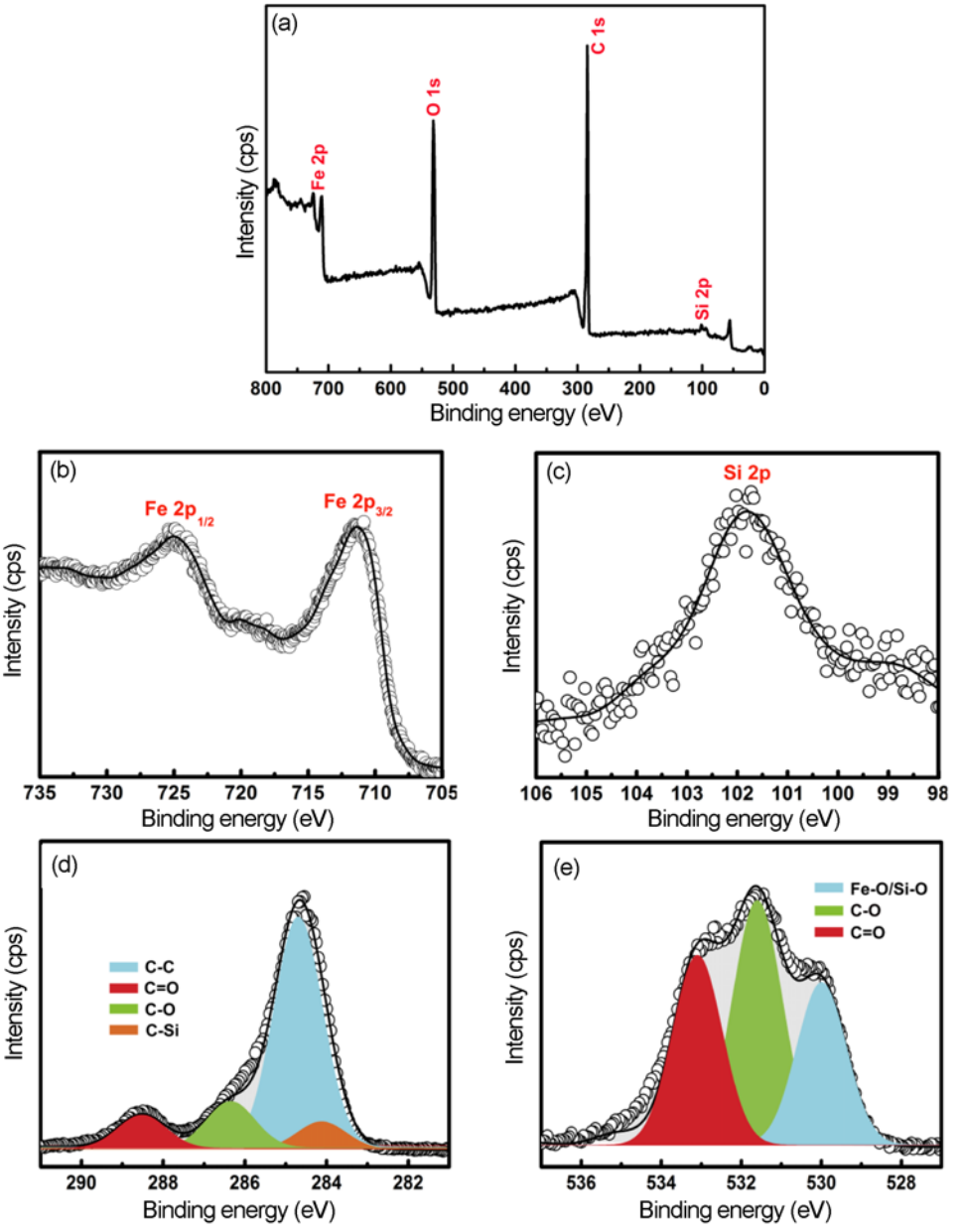

Figure 2. (a) XPS survey spectrum and high resolution XPS spectra of (b) Fe 2p, (c) Si 2p, (d) C 1s, (e) O 1s for Fe_3O_4/MPTMS/PAA nanocomposite. The experimental spectra were deconvolved into Gaussian components after Shirley background subtraction using CasaXPS software.

to these data, it was found that the nanoadsorbent dose affected Pb(II) uptake significantly. Increasing the nanoadsorbent dose from 0.2 g/*l* up to 1.0 g/*l* gave rise to a sharp increase in the Pb(II) removal percentage from 59.3±1.2 % to 97.5±0.8 %. This observation could be assigned to increased adsorption sites available. However, when the nanoadsorbent dose further increased from 1.0 g/*l*, the Pb(II) removal percentage levelled off, indicating an equilibrium had been established between the adsorbed Pb(II) and those dissociative in the solution. Based on these results, a nanoadsorbent dose of 1.0 g/*l* was selected for subsequent experiments.

The pH value that governed the dissociation degree of carboxyl groups and the hydrolysis of Pb(II) was another important factor affecting Pb(II) removal capability of the nanoadsorbent. Since Pb(II) cations (initial Pb(II) concentration= 5 mg/*l*, *T*=308 K) was inclined to precipitate as $Pb(OH)_2$ once the pH value exceeded 10 [26], the pH of interests herein was restricted to a range of 2.5-10. As could be seen in Figure 4(b), the Pb(II) removal percentage was only about 16 % when the pH value was 2.5. This phenomenon could

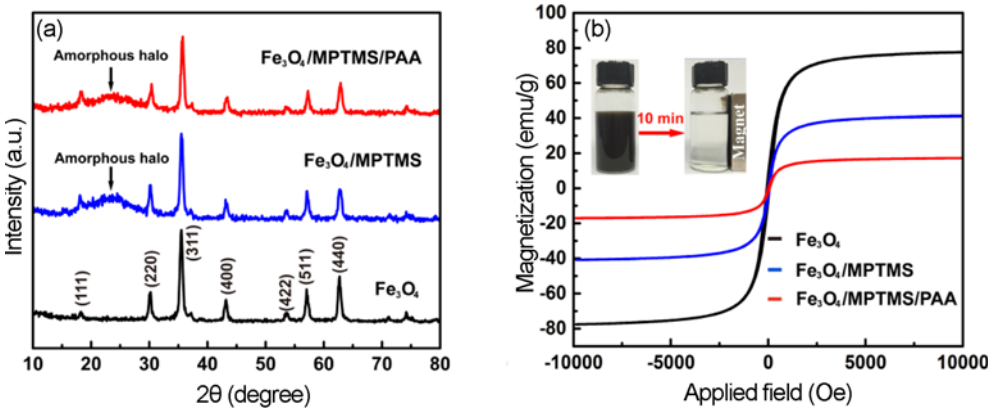

Figure 3. (a) XRD patterns and (b) room-temperature magnetic hysteresis loops of native Fe_3O_4, Fe_3O_4/MPTMS, and Fe_3O_4/MPTMS/PAA nanoparticles. The inset in (b) displays the appearance of 2.0 mg/m*l* Fe_3O_4/MPTMS/PAA nanocomposite dispersed in an aqueous solution of 0.1 M NaOH with a pH value of 8.0, and their fast response to an externally applied magnetic field.

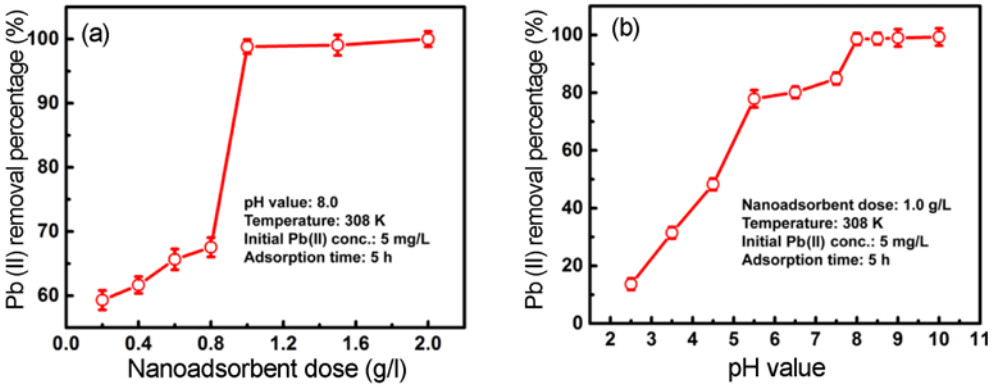

Figure 4. Effect of (a) nanoadsorbent dose and (b) pH value on Pb(II) removal percentage from aqueous solution using Fe_3O_4/MPTMS/PAA nanoadsorbent.

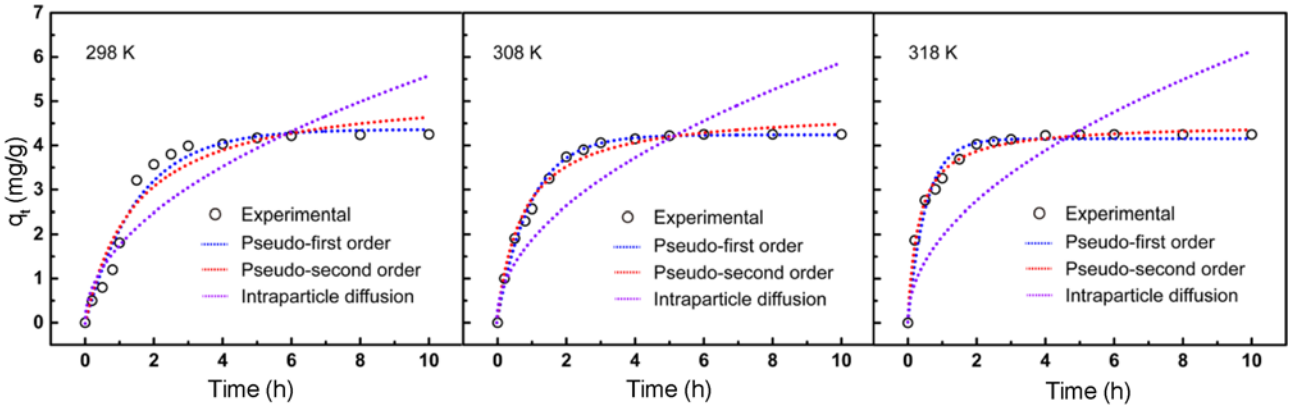

Figure 5. Kinetics of Pb(II) adsorption on Fe_3O_4/MPTMS/PAA nanoadsorbent at three different temperatures (Initial Pb(II) concentration= 5 mg/*l*; pH value=8.0; nanoadsorbent dose=1.0 g/*l*).

be ascribed to the fact that those carboxyl groups in PAA were predominantly undissociated, and thus uncoordinated with metal ions at such low pH value. As the pH value increased from 2.5 up to 8.0, the Pb(II) removal percentage increased significantly to approximately 97.9±1.1 %. On the one hand, this phenomenon could be attributed to increased dissociation degree of carboxyl groups in the PAA shell with increasing pH value. On the other hand, Pb(II) in aqueous

solution would gradually hydrolyze to form soluble hydroxide complexes, such as $Pb(OH)^+$, when the pH value increased up to 8.0. According to modern coordination chemistry, the presence of hydroxide ligands usually made dissociated carboxyls easily accessible to the metal center [27], which facilitated adsorption of Pb(II) cations. However, with the dissociation degree of carboxyl groups and the hydrolysis of Pb(II) approaching maximum at a pH value of 8.0, the Pb(II) removal percentage levelled off as the pH value increased thereafter. To guarantee as much Pb(II) could be removed as possible by Fe_3O_4/MPTMS/PAA nanoadsorbent, therefore, the pH value of the Pb(II) solution was set at 8.0 for all further experiments.

To better understand the adsorption process, the kinetic profiles of Pb(II) adsorption at three different temperatures were investigated, and the results were shown in Figure 5. It was found that regardless of the temperature, the Pb(II) removal rate was fast during the initial 2 h, followed by the adsorption approaching an equilibrium. The rapid Pb(II) adsorption by Fe_3O_4/MPTMS/PAA nanoadsorbent during the first stage was due to more adsorption sites accessible on the surface of the nanoadsorbent. This kinetics feature was beneficial for practice application, which saved the operating time of Fe_3O_4/MPTMS/PAA nanoadsorbent. In addition, pseudo-first order, pseudo-second order, and intraparticle diffusion models were employed to fit the experimental date in Figure 5, which shed light on possible adsorption mechanism of Pb(II) by Fe_3O_4/MPTMS/PAA nanoadsorbent. The equations for these three models were given in equations (3), (4) and (5), respectively [28]:

$$q_t = q_e \times (1 - e^{-k_1 \times t}) \tag{3}$$

$$q_t = \frac{t}{\frac{1}{k_2 \times q_e^2} + \frac{t}{q_e}} \tag{4}$$

$$q_t = k_3 \times \sqrt{t} \tag{5}$$

where q_t and q_e (mg/g) refer to the amount of Pb(II) adsorbed per unit adsorbent mass at time t (min) and at equilibrium, respectively; k_1 (min^{-1}), k_2 (g/mg min), and k_3 (mg/g $min^{1/2}$) stand for pseudo-first order, pseudo-second order and intraparticle diffusion rate constants, respectively. The fitting results by using non-linear regression were present in Table 1. For both pseudo-first order and pseudo-second order models, the average relative errors were relatively low (<3.45) and the coefficients of determination approached unity, indicating that these two models described well the kinetics data. In general, pseudo-first order approach is based on the conception that the adsorption rate is dominated by only one process or a mechanism involving a single class of adsorbing sites; pseudo-second order model assumes that the adsorption procedure may be a chemical one involving valence forces by the exchange or sharing of electrons between adsorbate and adsorbent [28,29]. Thus, it could be inferred that the Pb(II) adsorption process by Fe_3O_4/MPTMS/PAA nanoadsorbent was a chemical procedure involving valence forces *via* sharing or exchange of electrons, and the adsorption rate was limited by the availability of carboxyl groups only. Besides, it was found that k_1, k_2, as well as q_e from both pseudo-first order and pseudo-second order models were enhanced with increasing temperature, indicating the endothermic nature of the adsorption procedure.

Adsorption isotherm is often used to describe the relationship between the residual metal ion concentration in solution and the amount of metal adsorbed by solid phase at equilibrium, which reflects the efficiency of the adsorbents [30]. In the present study, Langmuir isotherm and Freundlich isotherm models were employed to fit the experimental equilibrium data obtained. The Langmuir isotherm hypothesizes that the adsorption can only take place at a fixed number of definite localized sites by chemical action [30]. Freundlich isotherm is an empirical isotherm assuming that the amount of adsorbate on the surface of the adsorbent enhances with adsorbate concentration [30]. The equations of these two models were formulated as follows [31]:

$$q_e = \frac{q_{\max} \times b \times C_e}{1 + b \times C_e} \tag{6}$$

$$q_e = K_F \times C_e^{1/n} \tag{7}$$

where q_e (mg/g) and C_e (mg/*l*) represent the adsorbate concentration in the solid and liquid phase at equilibrium, respectively; $q_{\max}$ (mg/g) and b (*l*/mg) are Langmuir constants that express the theoretical maximum for adsorbate adsorption and the affinity of the adsorbent, respectively; K_F ($(L/g)^{-1/n}$)

Table 1. Fitting results of Pb(II) adsorption on Fe_3O_4/MPTMS/PAA nanoadsorbent employing pseudo-first order, pseudo-second order, and intraparticle diffusion kinetic models

T (K)	Pseudo-first order				Pseudo-second order				Intraparticle diffusion		
	q_e (mg/g)	k_1 (min^{-1})	*ARE* (%)	R^2	q_e (mg/g)	k_2 (g/mg·min)	*ARE* (%)	R^2	k_3 (mg/g·$min^{1/2}$)	*ARE* (%)	R^2
298	4.14	0.66	2.12	0.96	4.48	0.13	3.45	0.93	1.77	8.92	0.78
308	4.24	1.03	0.98	0.99	4.81	0.28	2.79	0.99	1.85	10.11	0.63
318	4.38	1.90	2.00	0.95	5.33	0.69	2.35	0.99	1.93	18.20	0.17

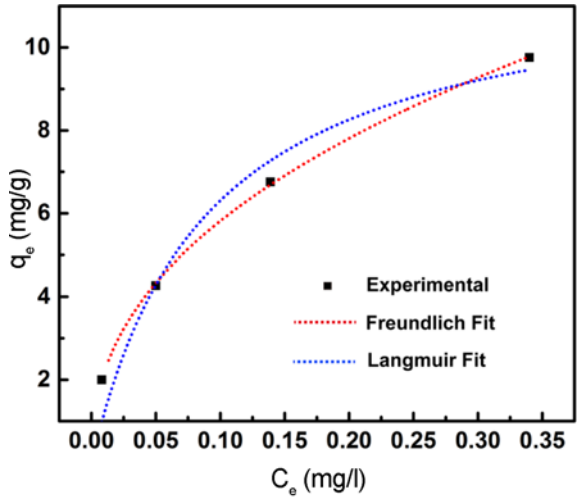

Figure 6. Adsorption isotherm of Pb(II) on Fe_3O_4/MPTMS/PAA nanoadsorbent (pH value=8.0; adsorption time=5 h; nanoadsorbent dose=1.0 g/*l*; temperature=308 K).

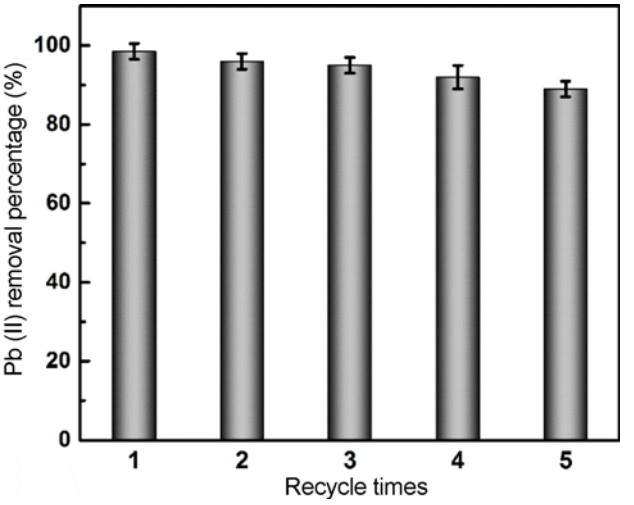

Figure 7. Pb(II) removal percentage of Fe_3O_4/MPTMS/PAA in different cycles (Initial Pb(II) concentration=5 mg/*l*; pH value=8.0; nanoadsorbent dose=1.0 g/*l*; temperature=308 K; adsorption time=5 h).

and *n* are Freundlich constants, referring to the adsorption capacity and intensity, respectively. Figure 6 exhibited the experimental equilibrium data, as well as the fitting results using Langmuir and Freundlich isotherm models. The parameters originating from the isotherm models were tabulated in Table 2. Clearly, both Langmuir and Freundlich isotherms provided a good correlation of the experimental equilibrium data since R^2>0.9. From Langmuir model, the theoretical maximum for metal uptake, q_{max}, could be obtained even if it could not be experimentally reached. The q_{max} value of Fe_3O_4/MPTMS/PAA nanoadsorbent for Pb(II) removal was 11.96 mg/g, comparable to other adsorbents that had been previously suggested efficient for Pb(II) removal from water (8.89 mg/g for bituminous coal [32]; 12.15-15.90 mg/g for sawdust [33]). According to the fitting results in Table 2, the K_F value of Fe_3O_4/MPTMS/PAA nanoadsorbent for Pb(II) removal was also comparable to those of other efficient Pb(II) adsorbents (11.49 for activated carbon [34]; 12.44 for sulphurised activated carbon [34]), indicating comparable adsorption capacity for a given adsorbate. In addition, the process of Pb(II) adsorption by Fe_3O_4/MPTMS/PAA nanoadsorbent was favorable according to the 1/*n* value (0.1<1/*n*<0.5, favorable; 1/*n*>2, unfavorable [35]).

From an economic perspective, it is important to regenerate the exhausted adsorbent for repeated use. As demonstrated in Figure 7, the Pb(II) removal percentage of Fe_3O_4/MPTMS/PAA nanoadsorbent slightly decreased when the regenerated nanoadsorbent was used repeatedly for Pb(II) removal. This phenomenon was quite normal in the reusability of adsorbents [36,37]. Despite such decrease, the Pb(II) removal percentage of Fe_3O_4/MPTMS/PAA nanoadsorbent was still over 90 % in the fifth adsorption-desorption cycles. Therefore, it was concluded that Fe_3O_4/MPTMS/PAA nanoadsorbent could be repeatedly used without compromising its adsorption potency significantly, promising its cost effectiveness as a nanoadsorbent for Pb(II)-containing water.

Conclusion

Polyacrylic acid could be grafted from Fe_3O_4 nanoparticle surface *via* the bridging function of MPTMS silane coupling agent. The components of the nanocomposite played synergistic roles as a nanoadsorbent for Pb(II) removal from contaminated water. The polyacrylic acid shell was capable of capturing Pb(II) *via* spontaneous, chemical coordination, while the magnetic core enabled fast separation of the exhausted nanoadsorbent from the decontaminated water by using a magnet. Pb(II) adsorption on such magnetite-supported nanoadsorbent was fast and efficient. By chemical desorption, the nanoadsorbent could be regenerated and reused without significantly compromising its original capability. Based on these advantages, the Fe_3O_4/MPTMS/PAA nanoadsorbent designed herein could be a potential

Table 2. Fitting results of Pb(II) adsorption isotherm on Fe_3O_4/MPTMS/PAA nanoadsorbent by Langmuir and Freundlich models

Langmuir isotherm model				Freundlich isotherm model			
q_{max} (mg/g)	*b* (*l*/mg)	*ARE* (%)	R^2	K_F (*l*/g)$^{1/n}$	1/*n*	*ARE* (%)	R^2
11.96	11.15	6.78	0.94	15.48	0.42	1.70	0.99

candidate for remediating Pb(II) contamination in water.

Acknowledgements

The authors gratefully acknowledge financial support of this work by Fundamental Research Funds for the Central Universities, China, Solid-state Fermentation Resource Utilization Key Laboratory of Sichuan Province (2015GTY012), and Sichuan University-ZSCHIMMER & SCHWARZ GmbH & Co. KG Scholarship.

Electronic Supplementary Material (ESM) The online version of this article (doi: 10.1007/s12221-016-6529-1) contains supplementary material, which is available to authorized users.

References

1. J. H. Jung, J. H. Lee, and S. Shinkai, *Chem. Soc. Rev.*, **40**, 4464 (2011).
2. X. Huang, C. Ke, and W. Wang, *Aquaculture*, **283**, 194 (2008).
3. C. M. L. Carvalho, E. Chew, S. I. Hashemy, J. Lu, and A. Holmgren, *J. Biol. Chem.*, **283**, 11913 (2008).
4. A. Dąbrowski, Z. Hubicki, P. Podkościelny, and E. Robens, *Chemosphere*, **56**, 91 (2004).
5. N. Meunier, P. Drogui, C. Montané, R. Hausler, G. Mercier, and J. F. Blais, *J. Hazard. Mater.*, **137**, 581 (2006).
6. S. M. C. Ritchie and D. Bhattacharyya, *J. Hazard. Mater.*, **92**, 21 (2002).
7. Y. Kikuchi, Q. Qian, M. Machida, and H. Tatsumoto, *Carbon*, **44**, 195 (2006).
8. R. K. Upadhyay, N. Soin, and S. S. Roy, *RSC Adv.*, **4**, 3823 (2014).
9. J. H. Jung, J. H. Lee, and S. Shinkai, *Chem. Soc. Rev.*, **40**, 4464 (2011).
10. G. A. Mansoori, "Principles of Nanotechnology: Molecular-based Study of Condensed Matter in Small Systems", World Scientific Publishing, Singapore, 2005.
11. R. P. Feynman, *Eng. Sci.*, **23**, 22 (1960).
12. A. Hoshino, K. Fujioka, T. Oku, M. Suga, Y. F. Sasaki, T. Ohta, M. Yasuhara, K. Suzuki, and K. Yamamoto, *Nano Lett.*, **4**, 2163 (2004).
13. T. Yu, J. Lin, J. Xu, T. Chen, and S. Lin, *Polymer*, **46**, 5695 (2005).
14. P. Xu, G. Zeng, D. Huang, C. Feng, S. Hu, M. Zhao, C. Lai, Z. Wei, C. Huang, G. Xie, and Z. Liu, *Sci. Total Environ.*, **424**, 1 (2012).
15. P. Xu, G. Zeng, D. Huang, C. Lai, M. Zhao, Z. Wei, N. Li, C. Huang, and G. Xie, *Chem. Eng. J.*, **203**, 423 (2012).
16. J. Liu, S. Z. Qiao, Q. H. Hu, and G. Q. Lu, *Small*, **7**, 425 (2011).
17. A. Lu, E. L. Salabas, and F. Schüth, *Angew. Chem. Int. Ed.*, **46**, 1222 (2007).
18. V. Polshettiwar, R. Luque, A. Fihri, H. Zhu, M. Bouhrara, and J. Basset, *Chem. Rev.*, **111**, 3036 (2011).
19. J. Chang, Y. Chen, S. Zhao, X. Guan, and H. Fan, *Polym. Chem.*, **6**, 8150 (2015).
20. M. Feng, R. Qu, X. Zhang, P. Sun, Y. Sui, L. Wang, and Z. Wang, *Water Res.*, **85**, 1 (2015).
21. Y. Jin, F. Liu, C. Shan, M. Tong, and Y. Hou, *Water Res.*, **50**, 124 (2014).
22. Y. Li, J. Lan, R. Guo, M. Huang, K. Shi, and D. Shang, *Fiber. Polym.*, **14**, 1657 (2013).
23. X. Guan, J. Chang, Y. Chen, and H. Fan, *RSC Adv.*, **5**, 50126 (2015).
24. M. Pooresmaeil, Y. Mansoori, M. Mirzaeinejad, and A. Khodayari, *Adv. Polym. Tech.*, DOI: 10.1002/adv.21665 (2016).
25. X. Guan, J. Chang, Z. Xu, Y. Chen, and H. Fan, *RSC Adv.*, **6**, 29054 (2016).
26. C. Weng, *J. Colloid Interface Sci.*, **272**, 262 (2004).
27. A. D. Covington, *Chem. Soc. Rev.*, **26**, 111 (1997).
28. A. B. Pérez Marín, M. I. Aguilar, V. F. Meseguer, J. F. Ortuño, J. Sáez, and M. Lloréns, *Chem. Eng. J.*, **155**, 199 (2009).
29. Y. Bulut and Z. Tez, *J. Hazard. Mater.*, **149**, 35 (2007).
30. A. B. Pérez-Marín, V. Meseguer Zapata, J. F. Ortuño, M. Aguilar, J. Sáez, and M. Lloréns, *J. Hazard. Mater.*, **139**, 122 (2007).
31. C. Hou, H. Yang, Z. Xu, and Y. Wei, *Fiber. Polym.*, **16**, 1917 (2015).
32. D. Singh and N. S. Rawat, *Ind. J. Chem. Technol*., **4**, 49 (1995).
33. B. Yasemin and T. Zek, *J. Environ. Sci.*, **19**, 160 (2007).
34. J. Goel, K. Kadirvelu, C. Rajagopal, and V. K. Garg, *J. Hazard. Mater.*, **B125**, 211 (2005).
35. D. D. Do, "Adsorption Analysis: Equilibria and Kinetics", Singapore: World Scientific, 1998.
36. W. Zhang, X. Shi, Y. Zhang, W. Gu, B. Li, and Y. Xian, *J. Mater. Chem. A*, **1**, 1745 (2013).
37. M. Bhaumik, A. Maity, V. V. Srinivasu, and M. S. Onyango, *J. Hazard. Mater.*, **190**, 381 (2011).